15

Wood Subjected to Hygro-Thermal and/or Mechanical Loads

Izet Horman, Dunja Martinović, Izet Bijelonja and Seid Hajdarević
Mechanical Engineering Faculty, University of Sarajevo
Bosnia and Herzegovina

1. Introduction

The FV method was originally developed for fluid flow, heat and mass transfer calculations (Patankar, 1980), and later generalized for stress analysis in isotropic linear and non-linear bodies (Demirdžić & Muzaferija, 1994; Demirdžić et al., 1997; Demirdžić & Martinović, 1993). For the purpose of the stress analysis in the wood, the method is modified to take into account the anisotropic nature of the wood and influence of the moisture content and the temperature on the deformation and stresses (Horman, 1999). Also, performance of the wood is found to be very sensitive to the moisture content and the temperature. Thus, it is of a great importance to be able to predict behavior of such materials under different hygro-thermo-mechanical loads. In order to demonstrate the methods capabilities, a transient analysis of fields of temperature, moisture, and stresses and displacement in the wood subjected to hygro-thermal or mechanical loads is performed.

2. Theory

2.1 Governing equations

The behaviour of an arbitrary part of a solid, porous body at any instant of time can be described by the following energy, mass and momentum balance equations which, when written in a Cartesian tensor notation, read:

$$\frac{\partial}{\partial t}\left(\rho c_q T\right) = -\frac{\partial q_j}{\partial x_j} + \rho s_q \tag{1}$$

$$\frac{\partial}{\partial t}\left(\rho c_m M\right) = -\frac{\partial \dot{m}_j}{\partial x_j} + \rho s_m \tag{2}$$

$$\frac{\partial}{\partial t}\left(\rho \frac{\partial u_i}{\partial t}\right) = \frac{\partial \sigma_{ij}}{\partial x_j} + \rho b_i\,, \qquad i = 1,2,3 \tag{3}$$

In these equation, t is time, x_i is the Cartesian coordinate, ρ is the mass density, c_q and c_m are the specific heat and the specific moisture, T is the temperature, M is the

moisture potential and u_i is the displacement, s_q and s_m are the heat and mass source, b_i is the body force, and q_j, $\dot{m}_j$ and σ_{ij} are the heat and mass flux vector, and stress tensor components, respectively.

2.2 Constitutive relations

In order to close the system of Eqs. (1)-(3) the constitutive relations for heat and mass flux based on the theory of Luikov (1966) which takes into account both the Soret and Duffort effect, together with the constitutive relation for a solid body are used:

- for Eqs. (1) and (2) heat and mass flux vector are

$$q_j = -k_{jl}^q \frac{\partial T}{\partial x_l} + \varepsilon r \dot{m}_j = -\left(k_{jl}^q + \varepsilon r \delta k_{jl}^m\right)\frac{\partial T}{\partial x_l} - \varepsilon r k_{jl}^m \frac{\partial M}{\partial x_l} \tag{4}$$

$$\dot{m}_j = -k_{jl}^m \frac{\partial M}{\partial x_l} - \delta k_{jl}^m \frac{\partial T}{\partial x_l} \tag{5}$$

- for an elastic, porous, orthotropic material for Eqs. (3) is

$$\sigma_{ij} = C_{ijkl}\,\varepsilon_{kl} - \alpha_{ij}\Delta T - <\beta_{ij}\Delta M> = \frac{1}{2}C_{ijkl}\left(\frac{\partial u_k}{\partial x_l} + \frac{\partial u_l}{\partial x_k}\right) - \alpha_{ij}\Delta T - <\beta_{ij}\Delta M> \tag{6}$$

Here k_{ij}^q and k_{ij}^m are the heat and mass conduction coefficient tensor components, respectively, ε is the ratio of the vapour diffusion coefficient to the coefficient of total diffusion of moisture, r is the heat of the phase change, δ is the temperature-gradient coefficient, ε_{ij} are the strain tensor components, C_{ijkl} are the elstic constant tensor components, α_{ij} are the coefficients of thermal expansion, β_{ij} are the shrinkage (contraction) coefficients, $\Delta T = T - T_u$, $\Delta M = M - M_h$ and T_u is the temperature at an udeformed state and M_h is the moisture potential at the fiber saturation point. For an orthotropic material and the coordinate axes aligned with the symmetry axes, Eqs. (4)-(6) can be written in the following matrix form:

$$\begin{bmatrix} q_1 \\ q_2 \\ q_3 \end{bmatrix} = -\begin{bmatrix} k_{11}^q + \delta\varepsilon r k_{11}^m & 0 & 0 \\ 0 & k_{22}^q + \delta\varepsilon r k_{22}^m & 0 \\ 0 & 0 & k_{33}^q + \delta\varepsilon r k_{33}^m \end{bmatrix}\begin{bmatrix} \frac{\partial T}{\partial x_1} \\ \frac{\partial T}{\partial x_2} \\ \frac{\partial T}{\partial x_3} \end{bmatrix} - \varepsilon r \begin{bmatrix} k_{11}^m & 0 & 0 \\ 0 & k_{22}^m & 0 \\ 0 & 0 & k_{33}^m \end{bmatrix}\begin{bmatrix} \frac{\partial M}{\partial x_1} \\ \frac{\partial M}{\partial x_2} \\ \frac{\partial M}{\partial x_3} \end{bmatrix} \tag{7}$$

$$\begin{bmatrix} \dot{m}_1 \\ \dot{m}_2 \\ \dot{m}_3 \end{bmatrix} = -\begin{bmatrix} k_{11}^m & 0 & 0 \\ 0 & k_{22}^m & 0 \\ 0 & 0 & k_{33}^m \end{bmatrix}\begin{bmatrix} \frac{\partial M}{\partial x_1} \\ \frac{\partial M}{\partial x_2} \\ \frac{\partial M}{\partial x_3} \end{bmatrix} - \delta \begin{bmatrix} k_{11}^m & 0 & 0 \\ 0 & k_{22}^m & 0 \\ 0 & 0 & k_{33}^m \end{bmatrix}\begin{bmatrix} \frac{\partial T}{\partial x_1} \\ \frac{\partial T}{\partial x_2} \\ \frac{\partial T}{\partial x_3} \end{bmatrix} \tag{8}$$

$$\begin{bmatrix}\sigma_{11}\\ \sigma_{22}\\ \sigma_{33}\\ \sigma_{12}\\ \sigma_{23}\\ \sigma_{31}\end{bmatrix}=\begin{bmatrix}A_{11} & A_{12} & A_{31} & 0 & 0 & 0\\ A_{12} & A_{22} & A_{23} & 0 & 0 & 0\\ A_{31} & A_{23} & A_{33} & 0 & 0 & 0\\ 0 & 0 & 0 & A_{44} & 0 & 0\\ 0 & 0 & 0 & 0 & A_{55} & 0\\ 0 & 0 & 0 & 0 & 0 & A_{66}\end{bmatrix}\begin{bmatrix}\varepsilon_{11}-\alpha_{11}\Delta T-<\beta_{11}\Delta M>\\ \varepsilon_{22}-\alpha_{22}\Delta T-<\beta_{22}\Delta M>\\ \varepsilon_{33}-\alpha_{33}\Delta T-<\beta_{33}\Delta M>\\ \varepsilon_{12}\\ \varepsilon_{23}\\ \varepsilon_{31}\end{bmatrix} \tag{9}$$

where the terms in $\langle\ \rangle$ brackets are „active" only for $M < M_h$, while the nine non-zero orthotropic elastic constants A_{ij} are related to the Young's moduli E_i, the Poisson's coefficients ν_{ij} and the shear moduli G_{ij} by the following relations:

$$A_{11}=\frac{E_1^2E_2E_3-\nu_{23}^2E_3^2E_1^2}{E_1E_2E_3\left(1-2\nu_{12}\nu_{23}\nu_{31}\right)-E_1^2E_2\nu_{31}^2-E_2^2E_3\nu_{12}^2-E_3^2E_1\nu_{23}^2},$$

$$A_{22}=\frac{E_1E_2^2E_3-\nu_{31}^2E_1^2E_2^2}{E_1E_2E_3\left(1-2\nu_{12}\nu_{23}\nu_{31}\right)-E_1^2E_2\nu_{31}^2-E_2^2E_3\nu_{12}^2-E_3^2E_1\nu_{23}^2},$$

$$A_{33}=\frac{E_1E_2E_3^2-\nu_{12}^2E_2^2E_3^2}{E_1E_2E_3\left(1-2\nu_{12}\nu_{23}\nu_{31}\right)-E_1^2E_2\nu_{31}^2-E_2^2E_3\nu_{12}^2-E_3^2E_1\nu_{23}^2},$$

$$A_{44}=2G_{12},\ A_{55}=2G_{23},\ A_{66}=2G_{31}, \tag{10}$$

$$A_{12}=\frac{\nu_{23}\nu_{31}E_1^2E_2E_3+\nu_{12}E_1E_2^2E_3}{E_1E_2E_3\left(1-2\nu_{12}\nu_{23}\nu_{31}\right)-E_1^2E_2\nu_{31}^2-E_2^2E_3\nu_{12}^2-E_3^2E_1\nu_{23}^2},$$

$$A_{23}=\frac{\nu_{31}\nu_{12}E_1E_2^2E_3+\nu_{23}E_1E_2E_3^2}{E_1E_2E_3\left(1-2\nu_{12}\nu_{23}\nu_{31}\right)-E_1^2E_2\nu_{31}^2-E_2^2E_3\nu_{12}^2-E_3^2E_1\nu_{23}^2},$$

$$A_{31}=\frac{\nu_{12}\nu_{23}E_1E_2E_3^2+\nu_{31}E_1^2E_2E_3}{E_1E_2E_3\left(1-2\nu_{12}\nu_{23}\nu_{31}\right)-E_1^2E_2\nu_{31}^2-E_2^2E_3\nu_{12}^2-E_3^2E_1\nu_{23}^2}.$$

Note that the pair of constitutive Equations (4) and (5) can be extended to take into account the effect of the pressure gradient on the heat and mass transfer.

- for a thermo-elasto-plastic isotropic material for Eqs (3) and (1) are

$$\delta\sigma_{ij}=2G\delta\varepsilon_{ij}+\lambda\delta_{ij}\delta\varepsilon_{kk}-(3\lambda+2G)\alpha\delta_{ij}\delta T-\left\langle\frac{3G\sigma_{ij}^d\sigma_{kl}^d\delta\varepsilon_{kl}}{\bar{\sigma}^2\left(\frac{H}{3G}+1\right)}\right\rangle \tag{11}$$

and constitutive relation (4) $\dot{m}_j=0$.

Here

$$\sigma_{ij}^{d} = \sigma_{ij} - \frac{1}{3}\delta_{ij}\sigma_{kk} \tag{12}$$

is the stress deviator and

$$\bar{\sigma} = \left(\frac{3}{2}\sigma_{ij}^{d}\sigma_{ij}^{d} \right)^{1/2} \tag{13}$$

is the effective stress (in the case of Von Mises yield criterion), G and λ are Lame's constants, α is the thermal expansion coeffifient, G is the shear modulus, H' is the plastic modulus, and δ_{ij} is the Kronecker delta.

Lame's constants are related to the more commonly used elastic modulus E and Poisson's coefficient ν by the following relationships:

$$\lambda = \frac{\nu E}{(1+\nu)(1-2\nu)}, \quad G = \frac{E}{2(1+\nu)} \tag{14}$$

In the case of elastic conditions, the expression within the brackets $\langle\ \rangle$ vanishes, and the constitutive realtion (11) reduces to the Duhamel-Neumann form of Hooke's law.

2.3 Initial and boundary conditions

In order to complete the mathematical model, initial and boundary conditions have to be specified. As initial conditions, the temperature, the moisture potential, and the displacement and velocity components have to be specified at all points of the solution domain.

For a wood heat treatment process, boundary conditions can be either of Dirichlet or Von Neuman type, i.e. temperature and/or heat flux and displacements and/or forces (surface tractions) have to be specified at all boundaries.

For a convective wood drying process, the following boundary conditions are normally appropriate:

$$k_{jl}^{q}\frac{\partial T}{\partial x_l}n_j + h_q\left(T - T_a\right) + \left(1-\varepsilon\right)rh_m\left(M - M_a\right) = 0$$

$$k_{jl}^{m}\frac{\partial M}{\partial x_l}n_j + h_m\left(M - M_a\right) + \delta k_{jl}^{m}\frac{\partial T}{\partial x_l}n_j = 0 \tag{15}$$

$$\sigma_{ji}n_j = f_{si}$$

where h_q and h_m are the (convective) heat and mass transfer coefficients, respectively, f_{si} is the surface traction, and all quantities are calculated at the solution domain boundary, except for those with subscript a which correspond to the ambient air.

3. Numerical method

3.1 Generic transport equation

Before the construction of a numerical algorithm is started, it is important to notice that the governing Eqs. (1)-(3) or Eqs. (1) and (3) when combined with constitutive Eqs. (7)-(9), or Eqs. (4) ($\dot{m}_j = 0$) and (11) can be written in the form of the following generic transport equation:

$$\frac{\partial}{\partial t}\left(\rho B_\psi\right) - \frac{\partial}{\partial x_j}\left(\Gamma_{jl}^{\psi}\frac{\partial \psi}{\partial x_l}\right) - S_\psi = 0\,, \qquad \left(\Gamma_{jl}^{\psi} = 0 \quad \text{for} \quad j \neq l\right) \tag{16}$$

which can be integrated over an arbitrary solution domain V bounded by the surface A, with unit outer normal vector n_j to yield:

$$\int_V \frac{\partial}{\partial t}\left(\rho B_\psi\right) dV - \int_A \Gamma_{jl}^{\psi}\frac{\partial \psi}{\partial x_l} n_j\, dA - \int_V S_\psi dV = 0\,, \quad \left(\Gamma_{jl}^{\psi} = 0 \ \text{ for } \ j \neq l\right) \tag{17}$$

The generic variable ψ stands for T, M or u_i.

The maeaning of the coefficients B_ψ, Γ_{jj}^{ψ} and S_ψ for the wood drying process is given in Table 1.

ψ	B_ψ	Γ_{11}^{ψ}	Γ_{22}^{ψ}	Γ_{33}^{ψ}	S_ψ
T	$c_q T$	$k_{11}^q + \varepsilon r \delta k_{11}^m$	$k_{22}^q + \varepsilon r \delta k_{22}^m$	$k_{33}^q + \varepsilon r \delta k_{33}^m$	$\frac{\partial}{\partial x_j}\left(\varepsilon r k_{jl}^m \frac{\partial M}{\partial x_l}\right) + \rho s_q$
M	$c_m M$	k_{11}^m	k_{22}^m	k_{33}^m	$\frac{\partial}{\partial x_j}\left(\delta k_{jl}^m \frac{\partial T}{\partial x_l}\right) + \rho s_m$
u_1	$\frac{\partial u_1}{\partial t}$	A_{11}	$\frac{A_{44}}{2}$	$\frac{A_{66}}{2}$	$\frac{\partial}{\partial x_1}\left(A_{12}\frac{\partial u_2}{\partial x_2} + A_{31}\frac{\partial u_3}{\partial x_3}\right) + \frac{\partial}{\partial x_2}\left(\frac{A_{44}}{2}\frac{\partial u_2}{\partial x_1}\right) + \frac{\partial}{\partial x_3}\left(\frac{A_{66}}{2}\frac{\partial u_3}{\partial x_1}\right) - \frac{\partial}{\partial x_1}\left[A_{11}\left(\alpha_{11}\Delta T + < \beta_{11}\Delta M >\right) + A_{12}\left(\alpha_{22}\Delta T + < \beta_{22}\Delta M >\right) + A_{31}\left(\alpha_{33}\Delta T + < \beta_{33}\Delta M >\right)\right] + \rho b_1$
u_2	$\frac{\partial u_2}{\partial t}$	$\frac{A_{44}}{2}$	A_{22}	$\frac{A_{55}}{2}$	$\frac{\partial}{\partial x_1}\left(\frac{A_{44}}{2}\frac{\partial u_1}{\partial x_2}\right) + \frac{\partial}{\partial x_2}\left(A_{12}\frac{\partial u_1}{\partial x_1} + A_{23}\frac{\partial u_3}{\partial x_3}\right) + \frac{\partial}{\partial x_3}\left(\frac{A_{55}}{2}\frac{\partial u_3}{\partial x_2}\right) - \frac{\partial}{\partial x_2}\left[A_{12}\left(\alpha_{11}\Delta T + < \beta_{11}\Delta M >\right) + A_{22}\left(\alpha_{22}\Delta T + < \beta_{22}\Delta M >\right) + A_{23}\left(\alpha_{33}\Delta T + < \beta_{33}\Delta M >\right)\right] + \rho b_2$
u_3	$\frac{\partial u_3}{\partial t}$	$\frac{A_{66}}{2}$	$\frac{A_{55}}{2}$	A_{33}	$\frac{\partial}{\partial x_1}\left(\frac{A_{66}}{2}\frac{\partial u_1}{\partial x_3}\right) + \frac{\partial}{\partial x_2}\left(\frac{A_{55}}{2}\frac{\partial u_2}{\partial x_3}\right) + \frac{\partial}{\partial x_3}\left(A_{31}\frac{\partial u_1}{\partial x_1} + A_{23}\frac{\partial u_2}{\partial x_2}\right) - \frac{\partial}{\partial x_3}\left[A_{31}\left(\alpha_{11}\Delta T + < \beta_{11}\Delta M >\right) + A_{23}\left(\alpha_{22}\Delta T + < \beta_{22}\Delta M >\right) + A_{33}\left(\alpha_{33}\Delta T + < \beta_{33}\Delta M >\right)\right] + \rho b_3$

Table 1. The meaning of $B_\psi, \Gamma_{jj}^{\psi}$ and S_ψ in Eqs. (16) and (17)

3.2 Finite volume discretisation

As all numerical methods, the present one consists of time, space and equations discretisation. The time interval of interest is subdivided into a number of subintervals δt, not necessarily of the the same length. The space is discretised by a number of contiguous, non-overlapping hexahedral control volumes (CV), with the computational points at their centres (Fig.1). Then the integrals in generic Equation (17) are calculated by employing the midpint rule, the gradients are evaluated by assuming a linear variation of the dependent variable ψ between the computational points, and a fully implicit temporal scheme is employed. As a result a non-linear algebraic equation of the following form for each CV is obtained:

$$a_P \psi_P - \sum_K a_K \psi_K = b \qquad (K = W, E, S, N, B, T) \tag{18}$$

where the coefficients a_K and b are defined as:

$$a_E = \left(\Gamma_{11}^{\psi}\right)_e \frac{A_e}{\delta x_{1e}} \text{ and similar expressions for other cell faces,}$$

$$a_P^o = \frac{V}{\delta t}\left(\rho \frac{B_\psi}{\psi}\right)_P^o, \qquad a_P = \sum_K a_K + a_P^o \quad , \qquad b = S_{\psi P}\, V + a_P^o \psi_P^o \tag{19}$$

where the subscripts P and e denote values at the centre of the CV and at the centre of the east cell-face, respectively, A_e is the area of the east cell face, V is the volume of the CV, δx_e is the distance between points P and E, and all quantities refer to the current time level, except for those with the superscript o which refer to the previous, „old" time level.

3.3 Solution algorithm

After assembling Eqs. (18) for all CVs and for all transport equations, five (four in 2D case) sets of N mutually coupled non-linear algebraic equations are obtained, where N is the number of CVs. Those equations are solved by employing the following segregated iterative procedure.

First, all dependent variables are given their initial values. Then the boundary conditions which correspond to the first time step are applied, and the sets of equations for each individual dependent variable (T, M, u_i) are linearised and temporarily decoupled by assuming that coefficient a_K and source terms b are known (calculated by using depedent variable values from the previous iteration or the previous time step), resulting in a system of linear algbraic equations of the form:

$$A_\psi \boldsymbol{\psi} = \mathbf{b}_\psi \tag{20}$$

for each dependent variable, where A_ψ is an N x N matrix, vector $\boldsymbol{\psi}$ contains values of depedent variable ψ at N nodal points and $\mathbf{b}_\psi$ is the source vector.

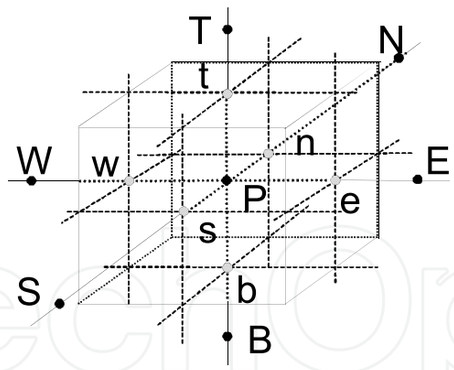

- Computational points
- Cell-face centres

Fig. 1. A typical control volume and the compass labelling scheme

Systems Eqs. (20) are then solved sequentially in turn until a converged solution is obtained. The procedure is assumed converged when the following conditions are satisfied for all five (four in 2D case) sets of equations:

$$\sum_{i=1}^{N} \left| a_P \psi_P - \sum_K a_K \psi_K - b \right| < pR_\psi \tag{21}$$

$$\left| \psi_i^m - \psi_i^{m-1} \right| < q \left| \psi_i^m \right| , \qquad i = 1,2,....,N$$

where p and q are typically of the order 10^{-3}, R_ψ is a suitable normalisation factor and superscripts m and $m-1$ denote values at two successive iterations.

In the next time step the whole procedure is repeated, except that the initial values are replaced by the values from the previous time step.

The present discretisation procedure ensures that the matrix A_ψ has the folowing desirable properties: it is seven (five in 2D case) – diagonal, symmetric, positive definite and diagonally dominant, which makes Eq. (20) easily solvable by a number of iterative methods which retain the sparsity of the matrix A_ψ. Note that it does not make sense to solve Eq. (20) to a tight tolerance since its coefficients and sources are only approximate (based on the values from the previous iteration/time step). Normally, reduction of the absolute residuals for one order of magnitude suffices.

The segregated solution strategy employed enables re-use of the same storage for the matrix A and vestor **b** for all depedent variables ψ, thus requiring only $8N$ storage locations ($6N$ in a 2D case). It is also important to mention that the fully implicit time differencing used, avoids stability-related time step restrictions. In principle, it allows any magnitude of the time step to be used, and in practice it is limited only by the required temporal accuracy.

When constitutive Eqs. (11) for a thermo-elasto-plastic isotropic material are applied, an elastic deformation is assumed at the beginning of iterations of each (load increment) time step (the expression within the brackets $\langle\ \rangle$ in Eqs. (11) is omitted). In the next iteration step in CVs in which the effective stress has reached the yield stress an elasto-plastic deformation is assumed and the expression within the brackets $\langle\ \rangle$ in Eqs. (11) is activated.

After each time step (load increment) displacements and stresses are updated adding displacement and stress increments in the current time step to the total displacements and total stresses from the previous time step. This procedure is repeated until the prescribed number of time steps (or load increments) is completed.

4. Application of the method

The method described in the previous sections has been applied to a number of both linear and non linear solid body deformation problems, few of which will be presented.

4.1 Numerical predictions of the wood drying process

The wood drying process is an important step in the manufacturing of wood products. During that process a non-uniform distribution of moisture content and temperature causes deformation and stresses in the wood and may result in a deformed and/or cracked end-product.

A wood drying process can be described as an unsteady process of heat, mass and momentum transfer in an orthotropic continuum with variable physical properties. The method solves a coupled set consisting of energy, moisture potential and momentum equations (1-3) with the constitutive relations (4-6).

Beech-wood beams (600x50x50 mm^3) are exposed to the uniform, unsteady flow of hot air in a laboratory dryer with an automatic control of the ambient air parameters (Horman, 1999).

The temperature and/or moisture dependent physical properties of the wood, obtained by fitting available experimental data, are given in Table 2. The others are considered constant and are given in Table 3. The timber is known to be cylindrically orthotropic. However, the wood samples used in this study are taken from the outer region of a cylindrical timber log and the rectilinear isotropy of samples is a reasonable assumption.

$E\,(Pa)$	C < 30 %	C ≥ 30 %
E_{11} (Pa)	$\left(6{,}69-4{,}66\,e^{-1{,}1\cdot 10^{7}\,C^{-6{,}3}}\right)\left(1{,}8-0{,}02T\right)10^{8}$	$2{,}05\left(1{,}8-0{,}02T\right)10^{8}$
E_{22} (Pa)	$\left(13{,}22-9{,}3\,e^{-2{,}5\cdot 10^{6}\,C^{-5{,}75}}\right)\left(1{,}8-0{,}02T\right)10^{8}$	$4{,}04\left(1{,}8-0{,}02T\right)10^{8}$
E_{33} (Pa)	$\left(81{,}11-57{,}03\,e^{-2{,}5\cdot 10^{6}\,C^{-5{,}75}}\right)\left(1{,}8-0{,}02T\right)10^{8}$	$24{,}79\left(1{,}8-0{,}02T\right)10^{8}$
ρ (kg/m^3)	$\dfrac{559(100+C)}{100-0{,}47(30-C)}$	$559\left(1+\dfrac{C}{100}\right)$
c_q (J/kg K)	$467\left[C(100+T)\right]^{0{,}2}$	
k_{11}^{q} (W/m K)	$1{,}36(0{,}088+0{,}000709T+0{,}00181C)$	
k_{22}^{q} (W/m K)	$1{,}15k_{11}^{q}$	

Table 2. Temperature and/or moisture dependent physical properties of wood ($C=c_m M$ (%) is the moisture content)

At the beginning of the drying process the wood samples had a uniform distribution of temperature, moisture, displacement and velocity:

$$T = 21\ °\text{C},\ M = 75\ °\text{M},\ u_i = \dot{u}_i = 0 \ \text{ for } \ t = 0\ .$$

Property	Value	Property	Value	Property	Value
r (J/kg)	$2{,}3 \cdot 10^{6}$	ν_{12}	0,36	α_{11} (1/K)	$37{,}6 \cdot 10^{-6}$
c_m (kg_m/kg°M)	0,01	ν_{21}	0,71	α_{22} (1/K)	$28{,}4 \cdot 10^{-6}$
k_{11}^m (kg_m/ms°M)	$4{,}5 \cdot 10^{-9}$	ν_{13}	0,043	α_{33} (1/K)	$4{,}16 \cdot 10^{-6}$
k_{22}^m (kg_m/ms°M)	$1{,}15\ k_{11}^m$	ν_{31}	0,52	β_{11} (1/°M)	$36{,}8 \cdot 10^{-4}$
G_{12} (Pa)	$3 \cdot 10^{8}$	ν_{23}	0.073	β_{22} (1/°M)	$18{,}0 \cdot 10^{-4}$
δ (°M/K)	2	ν_{32}	0,45	β_{33} (1/°M)	$1{,}8 \cdot 10^{-4}$

Table 3. Constant physical properties of wood

The coefficients of convective heat and mass transfer, based on the ambient air velocity of $v_a = 2$ m/s and moisture of $M_a = 10{,}5$ °M, were taken as:

$$h_q = 40\ \text{W/m}^2\text{K}, \qquad h_m = 1{,}8 \cdot 10^{-6}\ \text{kg/ m}^2\ \text{s°M},$$

while the ambient air temperature and the ratio of the vapour diffusion coefficient to the coefficient of total diffusion of moisture were assumed to vary during the drying process according to the following schedules:

$$T_a = \begin{cases} 28\ °\text{C} \\ 0{,}42\,t + 23.8 \\ 49\ °\text{C} \end{cases} \quad \text{for} \quad \begin{cases} 0 \le t \le 10 \\ 10 < t \le 60 \\ t > 60 \end{cases} \ \text{min} \qquad C_a = 10{,}5\ \%$$

$$\varepsilon = \begin{cases} 0{,}1 \\ 0{,}5 \\ 1{,}0 \end{cases} \quad \text{for} \quad \begin{cases} 0 \le t < 60 \\ 60 \le t < 3660 \\ t \ge 3660 \end{cases} \ \text{min}$$

Zero surface tractions are assumed and boundary conditions Eqs. (15) are applied.

For the purpose of the numerical calculations the problem is considered to be a 2D plane strain problem. Due to the double symmetry, only one quarter of the cross-section is taken as the solution domain. For all calculations presented in this study, a uniform numerical mesh consisting of 20 x 20 CV was employed, while the time step was varied from 10 to 100 min (first seven time steps of 10 min, 31 time steps of 30 min, and finally 140 time steps of 100 min). These results are found to be grid and time independent by performing a systematic grid and time-step refinement (difference between the results on the 20 x 20 CV mesh differ from ones obtained on a 40 x 40 CV mesh for less than 1%, while the results obtained with $\delta t = 3$ h practically coincide with results obtained with $\delta t = 1{,}5$ h).

During the initial phase of drying ($0 \le t < 2$ h) the moisture content is above the fiber saturation point and the deformation is a consequence of the thermal stress only. Figure 2 shows the calculated fields at $t = 70$ min. One can see that an increase in temperature (Fig. 2a) causes the expansion of wood sample (Fig. 2b) and that the outer region is subjected to compressive and the inner region to extensive stresses (Fig. 2c, d).

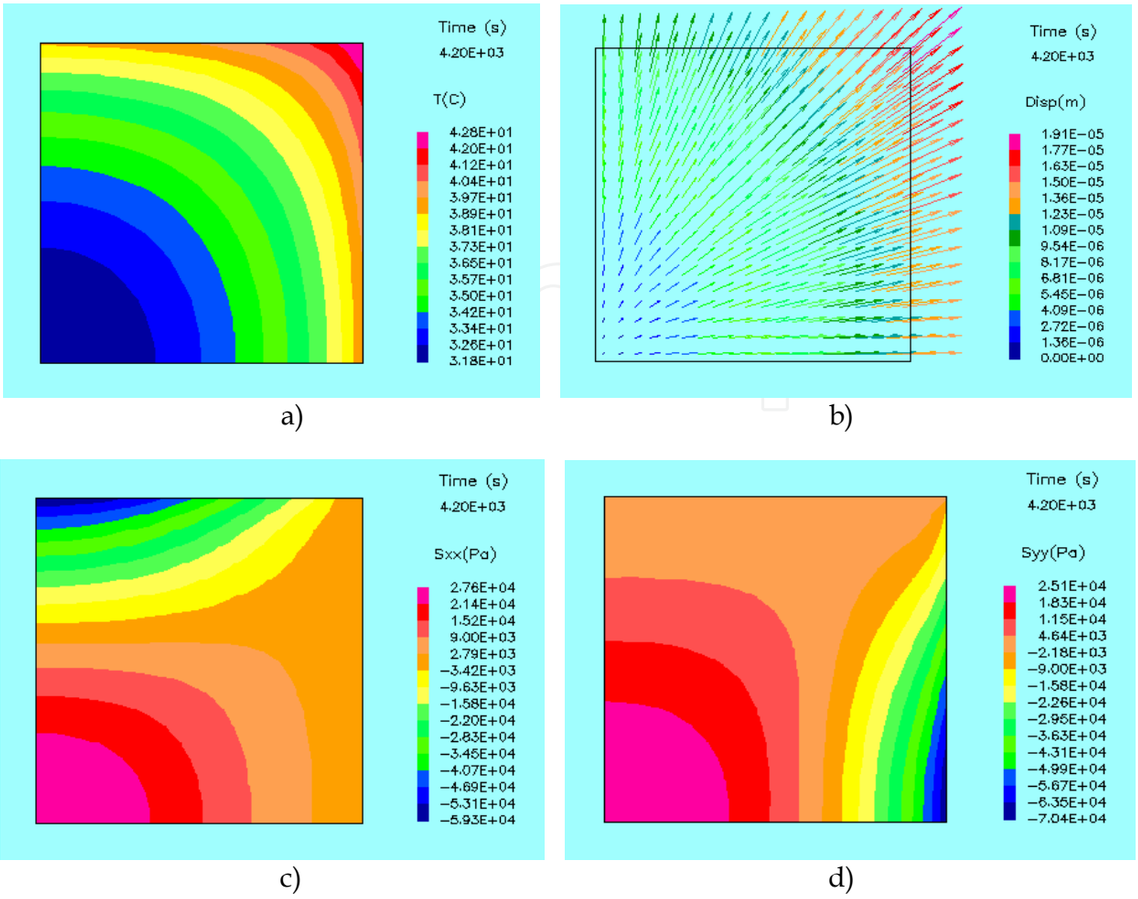

Fig. 2. Temperature (a), displacement (b), and normal stresses (c) and (d) at $t = 70$ min

During the period of intensive drying ($60 \le t < 190$ h) the deformation and stresses due to hygroscopic loads dominate. Figure 3 shows that at $t = 108$ h the moisture content has fallen below the fiber saturation point (Fig. 3a) and that this causes the shrinking of the wood sample (Fig. 3b). Around $t = 100$ h the stresses reach their maximum values and are extensive in the outer region and compressive in the interior of the sample (Fig. 3c, d). By comparing the values of stresses at $t = 70$ min and $t = 108$ h, it can be seen that the thermal stresses are around 200 times smaller than the stresses caused by the drop in the moisture content below the fiber saturation point.

If one plots the contours of the effective stress at $t = 108$ h, when it is at its maximum (Fig. 4), one can see that the effective stress is greater than the yield stress ($\sigma_y = 10$ MPa at 10% moisture; $\sigma_y = 6$ MPa at 30%) only in a very narrow surface region (1mm deep), which indicates that the plastic defomation did not take place in the interior of the sample, and that the drying schedule is well designed.

At the end of the drying process ($t = 246$ h), the moisture content in the sample varies from 11,1 to 14,4 % (Fig. 5a), while Fig. 5b and 5c illustrate the anisotropy of the wood sample, the contraction is 1,3 mm in the x and 0,6 mm in the y direction, or 6,5% and 3,3% (axis x and y).

In order to confirm the validity of the FV predictions, the calculated temperature, moisture and displacements are compared with experimental data (Horman, 1995., Institut für Holzphysik und mechanische Technologie des Holzes, Hamburg) at reference points (Fig. 6). Figures 7 and 8 show temperature and moisture content histories at two reference points. It can be seen a good agreement between calculations and experiment: maximum difference for both temperature and moisture was 8%, and the average difference was less than 2% (Martinović et al., 2001).

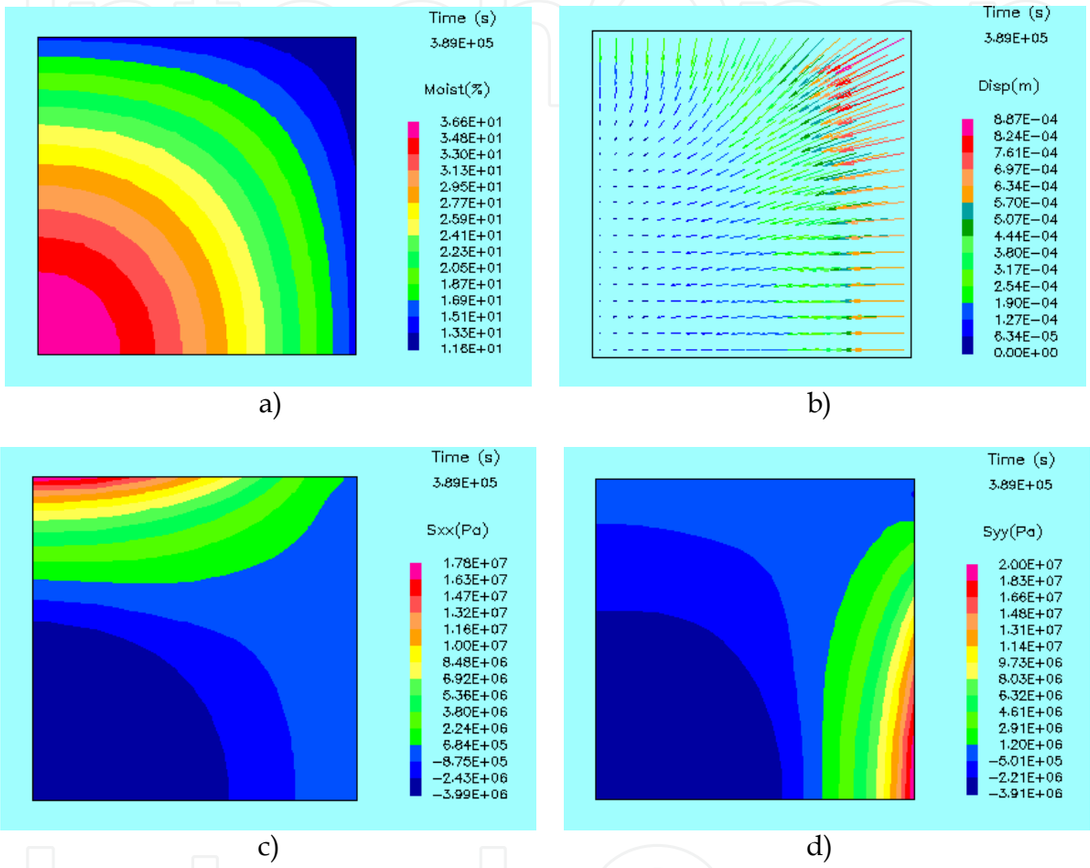

Fig. 3. Moisture (a), displacement (b), and normal stresses (c) and (d) at $t = 108$ h

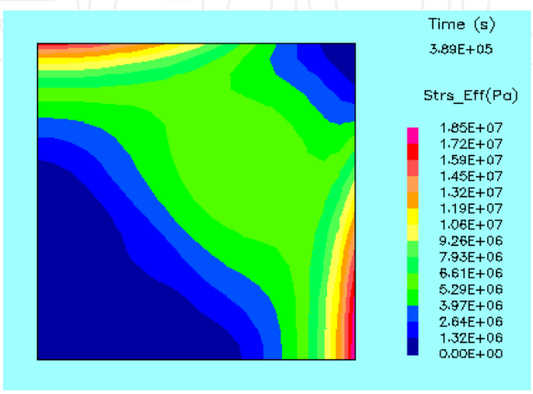

Fig. 4. Effective stress at $t = 108$ h

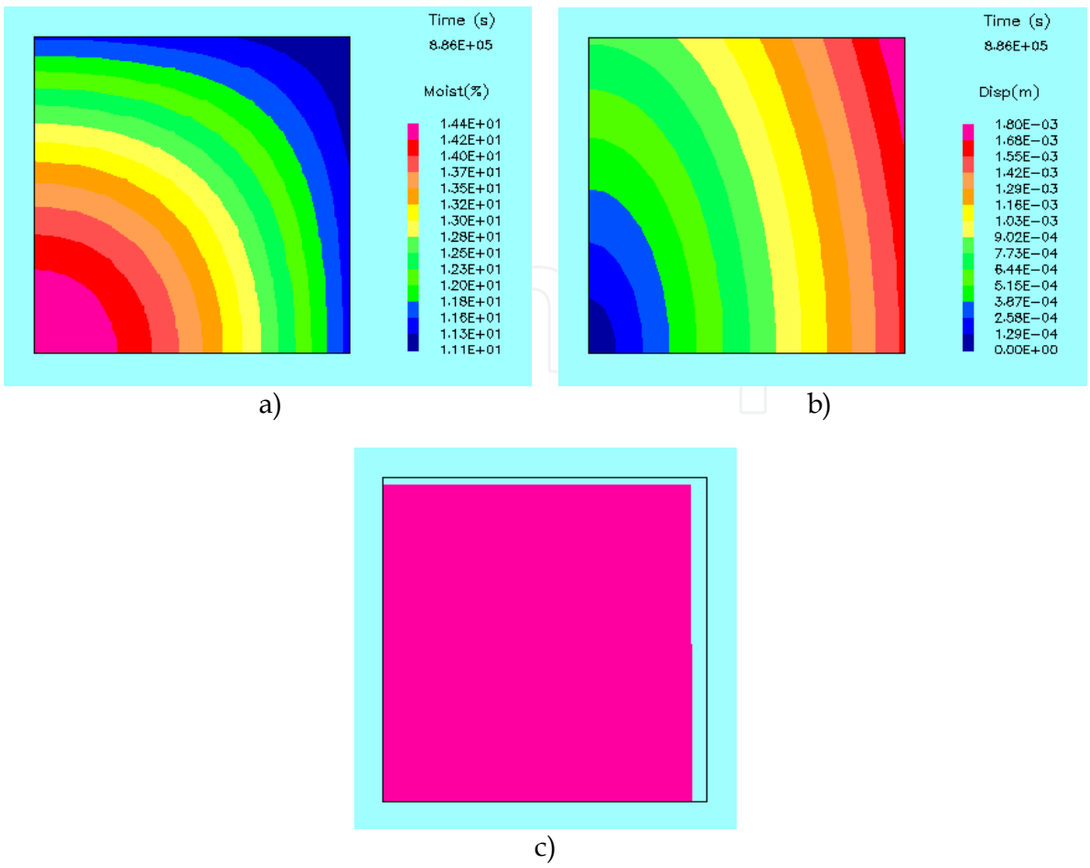

Fig. 5. Moisture (a), displacement (b), and cross section shape of deformed wood sample (one quarter of the cross section) contours at the end of drying schedule ($t = 246$ h)

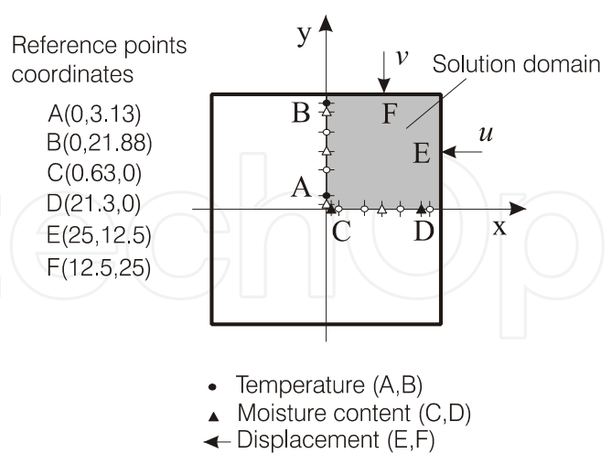

Fig. 6. Solution domain and reference points

Figure 9 shows how the displacements at two points on the surface of the sample vary during the drying process. One can see very little deformation during the initial phase ($t \leq 1000$ min) and a considerable shrinking of the sample afterwards, and that predictions closely follow experimental data (maximum difference 15%, average difference 5%).

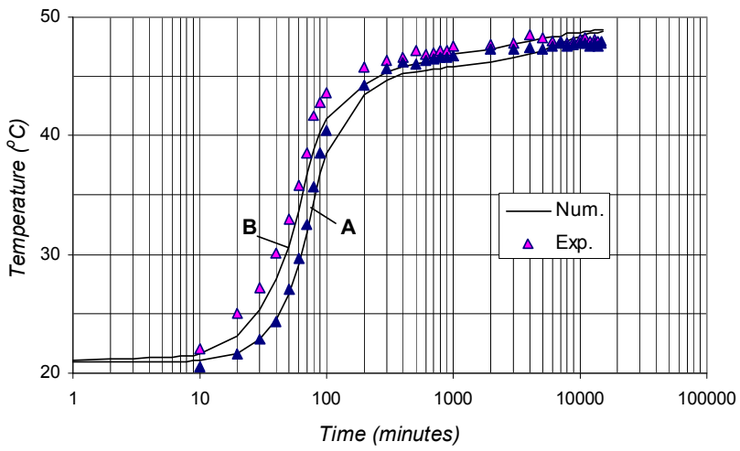

Fig. 7. Temperature history at reference points A and B

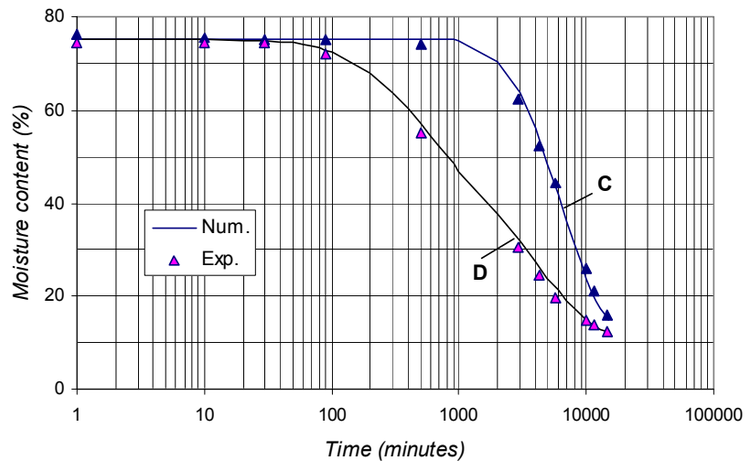

Fig. 8. Moisture content history at reference points C and D

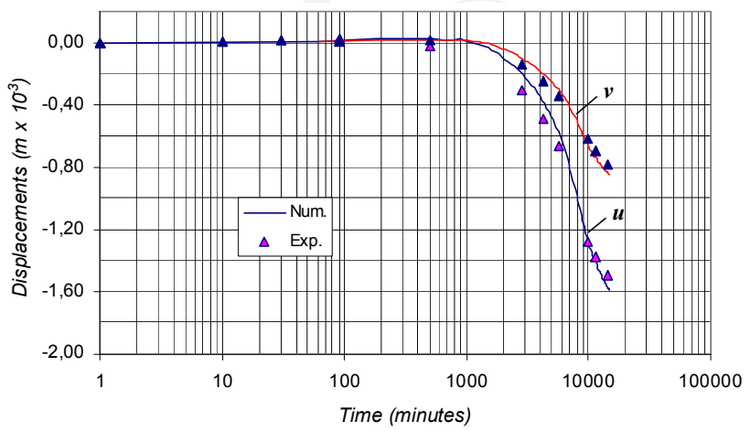

Fig. 9. u displacement at reference point E and v displacement at reference point F

4.2 Numerical predictions of the wood heat treatment process

The prediction of temperature, stresses and displacements in logs during their thermal preparation in the veneers production (wood steaming) is an important step for designing satisfying heating regime of logs preparation, without damaging in wood. The equations governing heat and momentum balance (Eqs. (1) and (3)) with corresponding constitutive relations (Eq. 11) in thermo-elasto-plastic material are solved.

For a mathematical description of a thermo-elasto-plastic deformation of the body the incremental plasticity theory is applied. The problem is considered to be a 2D plane strain problem (Horman et al., 2003).

A beech log with a diameter of 0,42 m and length of 5,1 m was exposed to steam, which temperature history during the phases of heating up, through-heating and cooling down is in Fig. 10 depicted. For numerical calculations the heat transfer coefficient $h_q = 7840\ \mathrm{W/m^2K}$, and thermal and mechanical properties of the wood given in Table 4 are used.

ρ	c	k	E	G	ν	α	σ_y
kg/m^3	J/kgK	W/mK	Pa	Pa	-	1/K	Pa
950	2950	0,54	$4{,}3 \cdot 10^8$	$1{,}6 \cdot 10^8$	0,35	$3{,}2 \cdot 10^{-5}$	$1{,}2 \cdot 10^6$

Table 4. Thermal and mechanical properties of wood ($c = 70\%$, $T = 80^o C$)

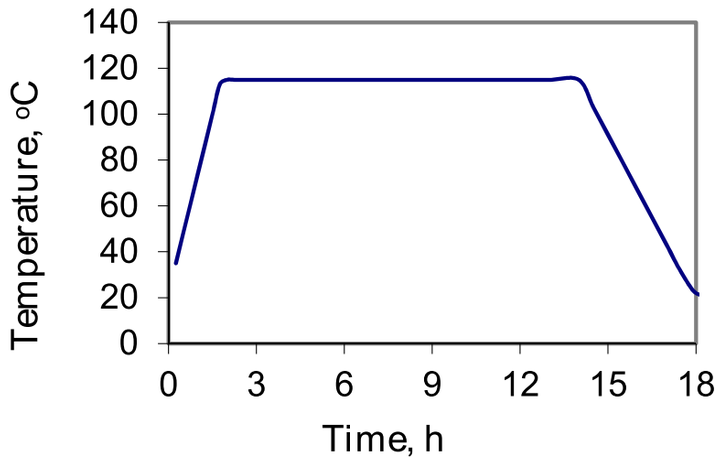

Fig. 10. Temperature history of the steam during the phases of heating up, through-heating and cooling down

Temporal temperature, radial displacement, and stress distributions at three points of the log cross section which is used for veneer production ($0{,}08m < r < 0{,}21m$) are shown in Figs. 11a-11d. In Figs. 12a and 12b effective stress distributions at three cross sections, and at four time values are depicted.

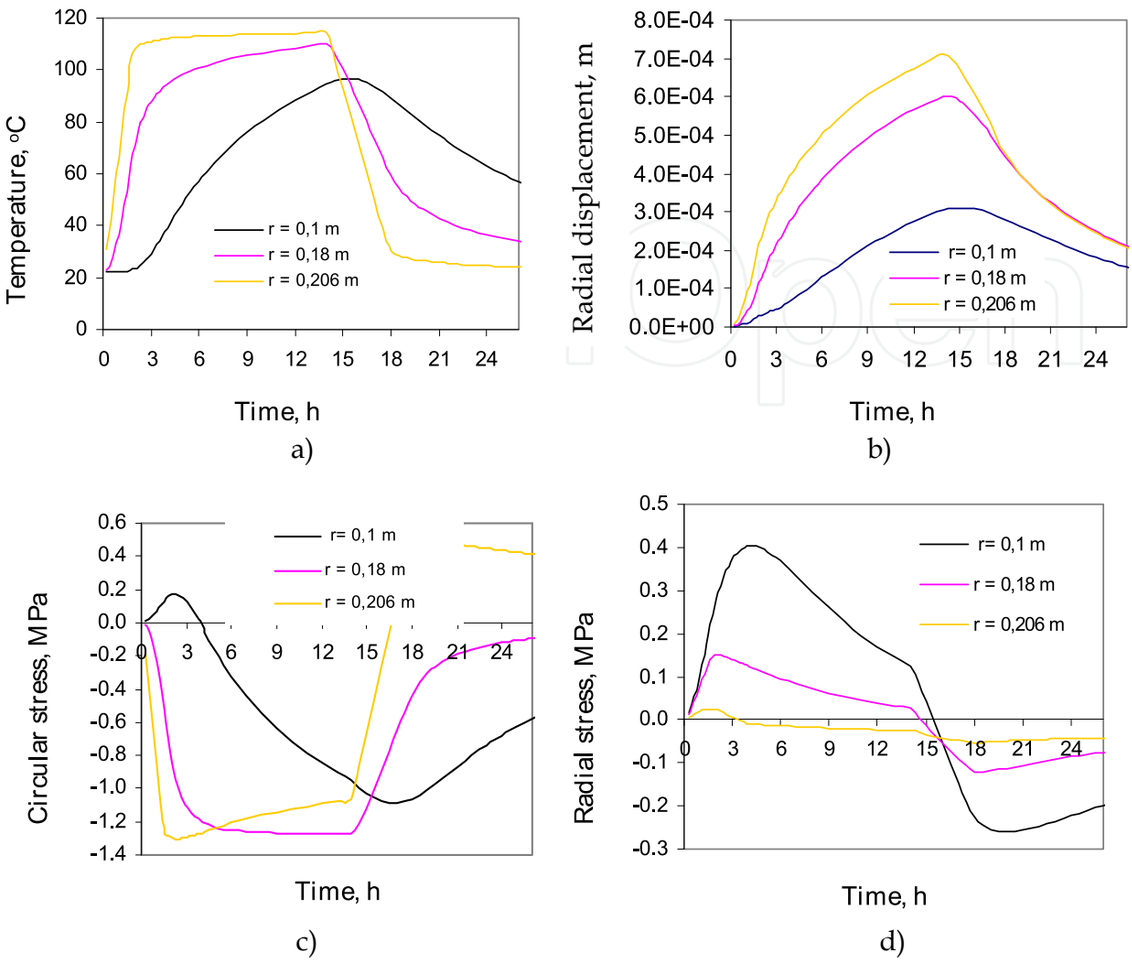

Fig. 11. Temporal a) temperature, b) radial displacement, c) circular stress, d) radial stress at three points of the log cross section $r_1 = 0{,}1$ m, $r = 0{,}18$ m i $r = 0{,}206$ m ($\varphi = const$) which is used for veneer production

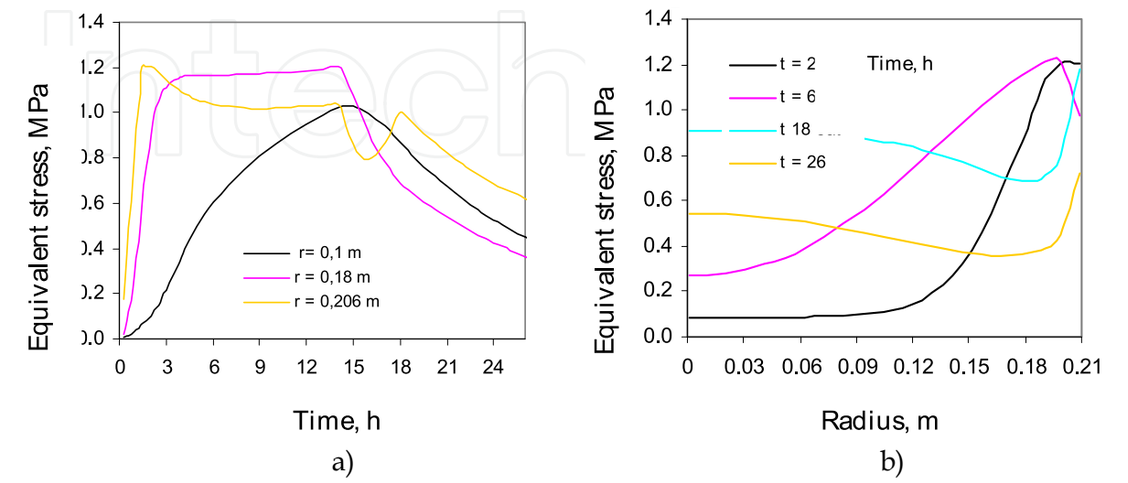

Fig. 12. Eeffective stress distributions a) at three cross sections, and b) at four time values

4.3 Numerical analysis of stress and strain conditions of a three-dimensional furniture skeleton construction and its joints

At the design stage of some pieces of furniture, their complex skeleton construction is subjected to stress and strain analysis. That allows them to satisfy all the functional demands (comfort), aesthetic demands, but also the strength and stiffness both by their shape and their dimensions. To achieve that, it is necessary to carry out a numerical simulation of the stress of a complex construction.

The finite volume method is used in the calculation. Orthotropy of the wood material is accounted for by approximating it with an isotropic material whose elastic modulus E and Poisson's ratio ν are calculated by employing the least-square method. The functional Q is minimized by E and ν (Martinović et al., 2008)

$$Q = \int_{sphere} \int_{0}^{2\pi} \left[\left(\sigma_{xx}^{ort} - \sigma_{xx}^{izo} \right)^2 + \left(\sigma_{yy}^{ort} - \sigma_{yy}^{izo} \right)^2 + \left(\sigma_{zz}^{ort} - \sigma_{zz}^{izo} \right)^2 + \left(\sigma_{xy}^{ort} - \sigma_{xy}^{izo} \right)^2 + \left(\sigma_{xz}^{ort} - \sigma_{xz}^{izo} \right)^2 + \left(\sigma_{yz}^{ort} - \sigma_{yz}^{izo} \right)^2 \right] d\alpha_x dA_{sphere} \tag{22}$$

and the obtained expressions are

$$E = \frac{(1+\nu)(1-2\nu)}{15(1-\nu)} \left[3(A_{xx} + A_{yy} + A_{zz}) + 2(A_{xy} + A_{xz} + A_{yz}) + 4(A_{kk} + A_{ll} + A_{mm}) \right] \tag{23}$$

$$\nu = \frac{A_{xx} + A_{yy} + A_{zz} + 4(A_{xy} + A_{xz} + A_{yz}) - 2(A_{kk} + A_{ll} + A_{mm})}{2\left[2(A_{xx} + A_{yy} + A_{zz}) + 3(A_{xy} + A_{xz} + A_{yz}) + (A_{kk} + A_{ll} + A_{mm}) \right]} . \tag{24}$$

The coefficients of the stiffness matrix A_{ij} are given in Eqs. (10).

The physical model is angle 3D joint and skeleton construction chair (Fig. 13.)

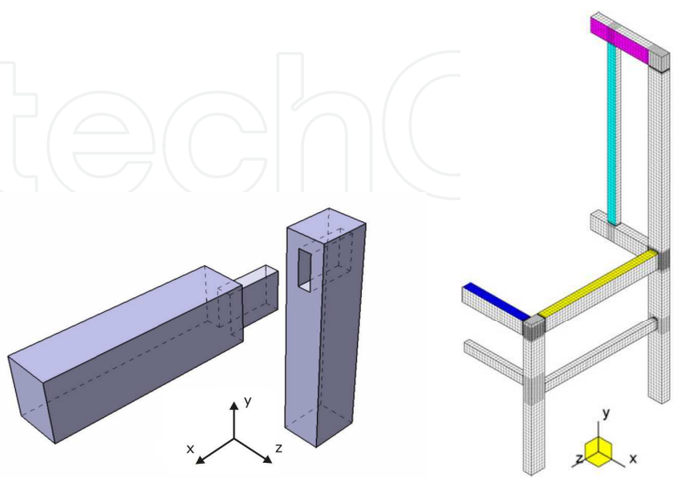

a) b)

Fig. 13. a) The angle joint, b) the model of an examined chair

Mechanical properties of wood, spruce, for temperature 20°C and moisture content 9,8 %, are given in Table 5. Mass density is 0,44 g/cm^3.

E_t	E_r	E_l	G_{rt}	G_{lr}	G_{lt}	ν_{tr}	ν_{rt}	ν_{rl}	ν_{lr}	ν_{tl}	ν_{lt}
GPa	GPa	GPa	GPa	GPa	GPa	-	-	-	-	-	-
0,392	0,686	15,916	0,0392	0,618	0,765	0,24	0,42	0,019	0,43	0,013	0,53

Table 5. Mechanical properties of wood, spruce

Elastic modulus and Poisson's ratio for the simulated isotropic material for 3D model (Eqs. (23) and (24)) are $E = 3,98$ GPa, and $\nu = 0,192$. The following assumptions and boundary conditions are used:

- angle joint is simplified; the glue line is neglected in a space,
- the force on the angle joint is exchanged with a uniform load.

Stress σ_{xx} and effective stress σ_{eff} contours are presented in Fig. 14.

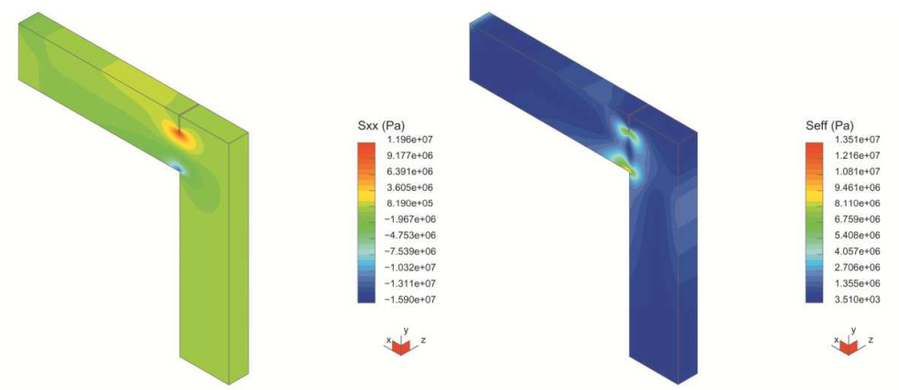

a) b)

Fig. 14. a) Normal stress σ_{xx} contours in the angle joint, b) effective stress σ_{eff} contours in the angle joint

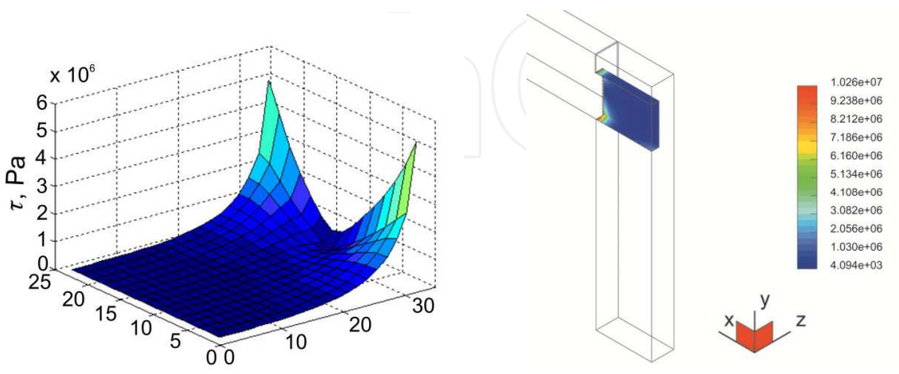

a) b)

Fig. 15. a) Tangential stress at the plane xy, at the distance of 4,6 mm from the symmetry plane b) tangential stress at the plane xy and resulting stress at the planes xz (the place of osculation of the planes of the tenon)

The highest value of the compressive stress σ_{xx} is in the symmetry plane, at undermost point of the tenon (~15,9 MPa), and the highest value of the tensile stress is at upper point of the tenon (~11,9 MPa). The place of the highest value of the effective stress is at the place of the highest compressive stress ($\sigma_{eff\,\max} = 13{,}5$ MPa). Tangential stress is presented on the plane xy at the distance of 4,6 mm from the symmetry plane. Figure 15a shows that the places of maximal stress ($\tau_{\max}$ ~5 MPa) are at $x = 35$ mm. At the same plane xy and the plane xz, in the place of osculation of the planes of the tenon, tangential stress and resulting stress (normal σ_{yy} and tangential stress τ_{yx}) are calculated, respectively and it are presented in Figure 15b. The maximal stress is ~ 10 MPa and it can be seen at the under part of the tenon.

In the end, the stress – strain analysis is done for the symmetrical half of the loaded chair (Horman et al., 2010). Mass load of the horizontal underframe of the whole chair is 100 kg and of the vertical frame is 22 kg. Effective stress contours at the elements of the chair frame and at the joints of the highest stresses ($\sigma_{eff\,\max}$ ~14 MPa) are presented in Figure 16.

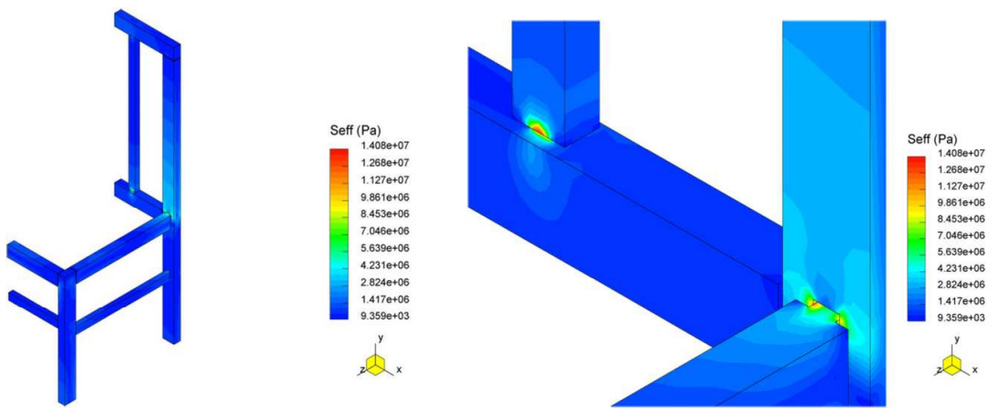

a) b)

Fig. 16. a) Distribution of effective stress at the skeleton chair, b) the joints of the highest stresses

Deformation of the chair is presented in Figure 17. The highest displacement is 13,3 mm.

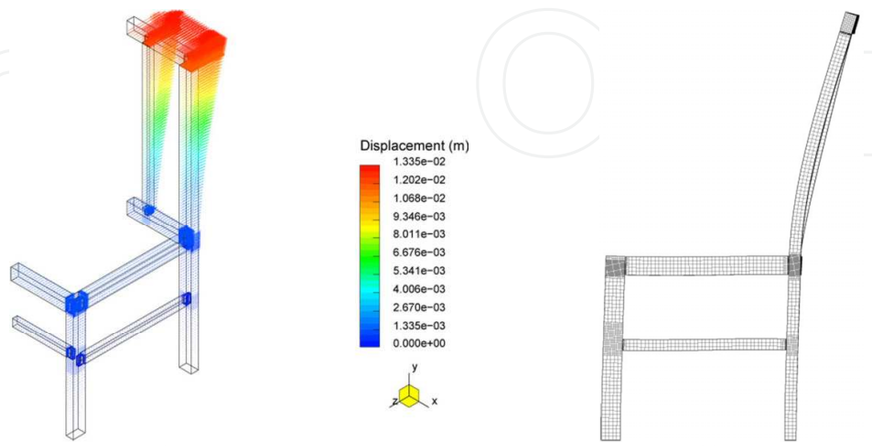

a) b)

Fig. 17. a) Distribution of displacements at the skeleton chair, b) deformed skeleton chair

5. Conclusion

The presented finite volume method for solution of the problems of energy, mass and momentum balance in conjugation with heat and mass transfer in an anisotropic, elasto-plastic, porous body is successful applied. Predictions of temperature, moisture content, strain and stress field in the wood drying as well as wood heat treatment process show high accurate results for course numerical grids due the second order accurate fully conservative spatial differencing scheme. The fully implicit unconditionally stable temporal differencing scheme enable large time steps during heat treatment processes. The applied finite volume discretisation procedure results in the diagonal dominant system of algebraic equations which are suitable for an iterative solution algorithm. The segregated iterative solution algorithm comprising the linearization and temporary decoupling of the system of equations for each dependent variable shows efficiency as well robustness solving highly nonlinear system of equations.

6. References

Demirdžić, I. & Martinović, D. (1993). Finite volume method for thermo-elasto-plastic stress analysis,*Comput. Methods Appl. Mech. Engrg.,* Vol 109, Issues. 3-4, (November 1993), pp. 331-349, ISSN 0045-7825

Demirdžić, I. & Muzaferija, S. (1994). Finite volume mtehod for stress analysis in complex domains, *Int. J. Numer. Methods Engrg.,* Vol 37, Issues. 21, (November 1994), pp. 3751-3766, ISSN 0029-5981

Demirdžić, I.; Muzaferija, S. & Perić, M. (1997). Benchmark solutions of some structural analysis problems using finite-volume mtehod and multigrid acceleration, *Int. J. Numer. Methods Engrg.,* Vol 40, Issues. 10, (May 1997), pp. 1893-1908, ISSN 0029-5981

Horman, I. (1999). *Finite volume method for analysis of timber drying,* PhD Thesis, University of Sarajevo (In Bosnian)

Horman, I.; Hajdarević, S.; Martinović, S. & Vukas, N. (2010). Numerical Analysis of Stress and Strain in a Wooden Chair, *Drvna industrija.,* Vol 61, No. 3, (September 2010), pp. 151-158, ISBN 0012-6772

Horman, I.; Martinović, D. & Bijelonja, I. (2003). Numerical Analysis Process of Wood Heat Treatment, *Proceedings of 4th International Scientific Conference of Production Engineering "RIM 2003"*, pp. 443-450, ISBN 9958-624-16-8, Bihać, Bosnia and Herzegovina, September 25-27, 2003

Luikov, A. V. (1966). *Heat and Mass Transfer in Capillary Porous Bodies,* Pergamon Press, Oxford, UK

Martinović, D.; Horman, I. & Demirdžić, I. (2001). Numerical and Experimental Analysis of a Wood Drying Process, *Wood Science and Technology,* Vol 35, No. 1-2, (April 2001), pp. 143-156, ISSN 0043-7719

Martinović, D.; Horman, I. & Hajdarević, S. (2008). Stress Distribution in Wooden Corner Joints, *Strojarstvo,* Vol 50, No. 4, (July-August 2008), pp. 193-204, ISBN 0562-1887

Patankar, S. V. (1980). *Numerical Heat Transfer and Fluid Flow,* McGraw-Hill, ISBN 0070487405, New York, USA

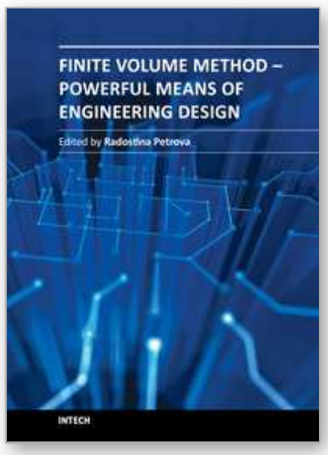

Finite Volume Method - Powerful Means of Engineering Design
Edited by PhD. Radostina Petrova

ISBN 978-953-51-0445-2
Hard cover, 370 pages
Publisher InTech
Published online 28, March, 2012
Published in print edition March, 2012

We hope that among these chapters you will find a topic which will raise your interest and engage you to further investigate a problem and build on the presented work. This book could serve either as a textbook or as a practical guide. It includes a wide variety of concepts in FVM, result of the efforts of scientists from all over the world. However, just to help you, all book chapters are systemized in three general groups: New techniques and algorithms in FVM; Solution of particular problems through FVM and Application of FVM in medicine and engineering. This book is for everyone who wants to grow, to improve and to investigate.

How to reference
In order to correctly reference this scholarly work, feel free to copy and paste the following:

Izet Horman, Dunja Martinović, Izet Bijelonja and Seid Hajdarević (2012). Wood Subjected to Hygro-Thermal and/or Mechanical Loads, Finite Volume Method - Powerful Means of Engineering Design, PhD. Radostina Petrova (Ed.), ISBN: 978-953-51-0445-2, InTech, Available from: http://www.intechopen.com/books/finite-volume-method-powerful-means-of-engineering-design/wood-subjected-to-hygro-thermal-and-or-mechanical-loads

INTECH
open science | open minds

InTech Europe
University Campus STeP Ri
Slavka Krautzeka 83/A
51000 Rijeka, Croatia
Phone: +385 (51) 770 447
Fax: +385 (51) 686 166
www.intechopen.com

InTech China
Unit 405, Office Block, Hotel Equatorial Shanghai
No.65, Yan An Road (West), Shanghai, 200040, China
中国上海市延安西路65号上海国际贵都大饭店办公楼405单元
Phone: +86-21-62489820
Fax: +86-21-62489821

IntechOpen